due to its continuous decomposition. It should, of course, be realized that the exact concentration of $Ru(CO)_5$ is unimportant for determination of rate constants of CO addition reactions since these are run under pseudo-first-order conditions. As a comparison, the rate constant for formation of $Fe_2(CO)_8$ in the gas phase is of similar magnitude, $\sim 10^{-9}$ cm^3 molec^{-1} s^{-1}.[27] Rate constants for formation of dinuclear metal carbonyl species tend to be larger than those for the reaction of the monometallic photofragments with CO.

$Ru(CO)_4$ Geometry. The lowest energy geometry for $Ru(CO)_4$ is predicted as D_{2d}, with C_{2v} as the next most favorable.[10] The overlap of infrared bands makes determination of photofragment geometry a difficult problem. As both symmetries have two IR active modes, isotopic labeling would be necessary to determine the structure unambiguously. These experiments are beyond the scope of this report.

IV. Conclusions

Photolysis of gas-phase $Ru(CO)_5$ with UV (248 and 351 nm) radiation produces $Ru(CO)_3$ and $Ru(CO)_4$. These fragments recombine with CO with rate constants $(7.6 \pm 0.3) \times 10^{-11}$ and $(2.8 \pm 0.8) \times 10^{-11}$ cm^3 molec^{-1} s^{-1}, respectively, which are both within approximately an order of magnitude of the gas kinetic rate constant. In addition, $Ru(CO)_4$ reacts with parent to form $Ru_2(CO)_9$. The reactivity of $Ru(CO)_4$ is markedly different from $Fe(CO)_4$. Recombination of $Fe(CO)_4$ with CO occurs at a rate $\sim 10^3$ slower than the ruthenium analogue because the reaction of $Fe(CO)_4$ with CO is spin-forbidden. The photoproducts of $Ru(CO)_5$ at 248 nm are almost exclusively $Ru(CO)_3$ and $Ru(CO)_4$. More $Ru(CO)_4$ is formed with 351-nm irradiation, but significant amounts of $Ru(CO)_3$ are also observed. Since the predominant products in $Fe(CO)_5$ photolysis are $Fe(CO)_2$ at 248 nm and $Fe(CO)_3$ at 351 nm, the average bond dissociation energies for the loss of three CO ligands from ruthenium are expected to be greater than that for the corresponding Fe–CO bonds. The first and second bond dissociation energies for sequential CO loss from $Ru(CO)_5$ appear to be similar and close to average, whereas the first and second CO bond dissociation energies for $Fe(CO)_5$ are considered to be significantly higher and lower respectively than the average for M–CO bonds. The relative instability of $Ru(CO)_5$ versus $Fe(CO)_5$ toward decomposition to the $[M(CO)_4]_3$ species can be rationalized on this basis.

Acknowledgment. We thank the National Science Foundation for support of this work under NSF Grant No. CHE 88-06020, and we acknowledge support of the donors of the Petroleum Research Fund administered by the American Chemical Society under Grant No. 18303-AC6, 3-C. The experimental assistance of Steven Gravelle was greatly appreciated.

(27) Ryther, R.; Weitz, E., to be published.

Collision-Induced Dissociation of Niobium Cluster Ions: Transition Metal Cluster Binding Energies

S. K. Loh,[†] Li Lian,[‡] and P. B. Armentrout*[,‡,§]

Contribution from the Departments of Chemistry, University of California, Berkeley, California 94720, and the University of Utah, Salt Lake City, Utah 84112.
Received October 21, 1988

Abstract: The cross sections for collision-induced dissociation (CID) of Nb_n^+ (n = 2–6) with Xe are presented. Experiments are conducted on a recently constructed guided ion beam mass spectrometer, which produces intense beams of thermalized, mass-selected, niobium cluster ions. Nb_n^+ are observed to fission to all possible ionic fragments and the largest possible neutral fragments at collision energies <10 eV. Evidence is presented for loss of multiple Nb atoms from the cluster at energies higher than 10 eV. This fragmentation pattern differs markedly from that previously observed for small iron cluster ions. CID thresholds are used to derive $D°(Nb_{n-1}^+–Nb)$ for n = 2–6, along with $D°(Nb_m)$ and ionization potentials (IPs) of Nb_m for m = 2 and 3. By using known IPs, $D°(Nb_n)$ for n = 4, 5, and 6 are also obtained. Nb_2^+ is found to be the most strongly bound cluster ion, $D°(Nb^+–Nb) = 6.15 \pm 0.15$, and Nb_3^+ is the most weakly bound cluster ion, $D°(Nb_2^+–Nb) = 4.60 \pm 0.15$ eV.

I. Introduction

Metal clusters constitute a new and exciting regime of matter, affording the opportunity to study changes in metal chemistry as a function of the number of metal atoms. Studies of transition-metal clusters are potentially applicable to an understanding of catalysis and oxidation processes that occur on surfaces or surface imperfections. Such studies in the gas phase can be used to probe the reactivity of the bare cluster, in the absence of complicating solvent effects. More complex processes can then be simulated by ligating the cluster and carrying out analogous reactions. Within the last 10 years, technological developments have made gas-phase studies possible.[1] Now, the information needed to quantitatively characterize cluster chemistry is beginning to accumulate.

Bond dissociation energies (BDEs) of clusters are important pieces of information that have gone largely uncharacterized. These are quantities that are essential to an understanding of reaction thermochemistry, since many reactions involve metal–metal bond cleavage and formation of new bonds with the reactant molecule. Although quantitative BDE measurements have been made on all first-row and many second-row transition-metal dimers,[2] such experimental work on larger gas-phase main-group metal[3,4] and transition-metal[5,6] clusters is scarce. All previously

[†] University of California.
[‡] University of Utah.
[§] Author to whom correspondence should be addressed. NSF Presidential Young Investigator, 1984–1989; Alfred P. Sloan Fellow; Camille and Henry Dreyfus Teacher-Scholar, 1988–1993.

(1) Dietz, T. G.; Duncan, M. A.; Powers, D. E.; Smalley, R. E. *J. Chem. Phys.* **1981**, *74*, 6511. Bondybey, V. E.; English, J. H. *J. Chem. Phys.* **1982**, *76*, 2165.
(2) Morse, M. D. *Chem. Rev.* **1986**, *86*, 1049.
(3) See for examples: Hanley, L.; Anderson, S. L. *J. Phys. Chem.* **1987**, *91*, 5161. Ruatta, S. A.; Anderson, S. L. *J. Chem. Phys.* **1988**, *89*, 273.
(4) Jarrold, M. F.; Bower, J. E. *J. Chem. Phys.* **1987**, *87*, 1610. Jarrold, M. F.; Bower, J. E. *J. Am. Chem. Soc.* **1988**, *110*, 70.
(5) Brucat, P. J.; Zheng, L.-S.; Pettiette, C. L.; Yang, S.; Smalley, R. E. *J. Chem. Phys.* **1986**, *84*, 3078.
(6) Loh, S. K.; Lian, L.; Hales, D. A.; Armentrout, P. B. *J. Chem. Phys.* **1988**, *89*, 610.

0002-7863/89/1511-3167$01.50/0

conducted studies have concentrated on ionic clusters. One reason is that cluster ions of a single mass (and size) can be selected by mass spectrometric techniques for study from the complex mixture of masses invariably formed during the clustering process. Another is that the velocities and trajectories of the ions can be controlled precisely. Ions are also easily detected, thus cluster reactions and cluster fragmentation processes can be followed unambiguously to products.

In the case of niobium (which has five valence electrons), the neutral dimer has been examined by ab initio calculation and by experimental methods. Complete active-space self-consistent-field (CASSCF) calculations on Nb_2 have been carried out by Walch and Bauschlicher.[7] The ground state was determined to be $^3\Sigma_g^-$ with a $5s\sigma$ bond and substantial 4d–4d interactions. Three states, $^1\Sigma_g^+$, $^1\Gamma_g$, and $^3\Delta_g$, are found to be within 0.12 eV of the ground state. Gupta and Gingerich have performed Knudsen cell studies,[8] obtaining $D°(Nb_2) = 5.57 \pm 0.41$ and 5.22 ± 0.02 eV by second and third law treatments, respectively. The latter has been revised in light of a new bond length and electronic degeneracies consistent with V_2 to be 4.86 ± 0.02 eV.[2] Several empirical and semi-empirical theoretical studies have also provided a wide range of bond energies, 3.85 to 5.2 eV.[9-11] Consideration of all of these results leads to the currently accepted value with rather wide error bars, $D°(Nb_2) = 5.0 \pm 0.40$ eV.[2]

We are aware of only three studies that have addressed the BDEs of larger niobium species. In the first, photofragmentation was used to bracket Nb_n^+ BDEs. Brucat et al. used the observation of single photon dissociation processes to bracket $D°(Nb_{n-1}^+-Nb) < 2.33$ eV ($n = 3$–10).[5] Note that these BDEs are considerably lower than $D°(Nb_2) \simeq 5.0$ eV. Single photon dissociation of Nb_2^+ was not observed, implying $D°(Nb^+-Nb) > 2.33$ eV. The lowest energy dissociation pathway was found to be production of Nb_{n-1}^+, or loss of an Nb atom. Using REMPI, the dipole-allowed states of the neutral clusters were found to be sparse up to 2 eV above the ground state. Cole, Liu, and Riley (CLR) have also examined Nb_n ($n = 5$–30) by photoionization and metastable decay in a time-of-flight mass spectrometer.[12] CLR found that one 5.0-eV photon was insufficient energy to ionize and fragment Nb_n, but they attribute such processes to multiple photon events. Under these conditions, Nb_n^+ dissociates to $Nb_{n-1}^+ + Nb$ ($n = 5$–14), but for $n = 15$–30, fission to other ionic fragments becomes dominant. Cole and Liu have performed further experiments on Nb clusters of six or more atoms.[13] It was found that metastable cluster fragmentation is source condition dependent. The cause for these observations is that these larger Nb clusters are in the form of metastable isomers. It was also found that fragmentation of large Nb_n^+ to Nb_p^+ ($p = 6$–11) can occur with the absorption of a single 3- to 4-eV photon.

In this paper, ion beam techniques are used to obtain thermochemical and kinetic information on Nb_n^+ ($n = 2$–6). Collision-induced dissociation (CID) of these clusters with Xe is presented. Cross sections, measured as a function of collision energy, are analyzed to provide both ionic and neutral cluster BDEs and the cluster ionization potentials (IPs). The mechanism for dissociation is also determined from the qualitative behaviors of the cross sections and the relative energy thresholds.

II. Experimental Section

Invariably, cluster BDEs are determined by breaking cluster bonds as a function energy. Internal energy can be transferred into the cluster by absorption of a photon or, as transpires here, by collision with an inert gas. In either case, fragmentation can occur only when the cluster internal energy exceeds the BDE. Therefore to obtain an accurate measure of the BDE, the clusters must start with a well-defined internal energy. In practice, this means that the clusters should be either spectroscopically cold or thermalized. Consequently, the means of cluster formation has been found to be very important. For example, cluster ions that experience $>10^4$ collisions with He followed by a supersonic expansion are observed to be cold.[5] In contrast, dimer (and probably larger cluster) ions created by photoionization of cold neutral clusters are vibrationally (and possibly electronically) excited. Metal cluster ions formed by FAB or SIMS techniques have even higher internal energies.[14]

The experiments described in this paper were performed on a recently constructed guided ion beam instrument, designed to make and study cold, mass-selected cluster ions. A complete description of the design and operation of the apparatus has been given in a recent publication,[15] so only a brief description follows here. Niobium cluster ions are created directly by laser vaporization of a niobium sample. Clustering occurs by condensation in a flow of helium carrier gas. We have implemented a copper vapor laser, with a high repetition rate (7 kHz) and high average power (25 W), to sputter a 6.35 mm diameter niobium rod. The rod rotates and translates to continuously expose the focussed laser spot to fresh niobium. The rate of vaporization also requires a continuous flow of He (6000 sccm) to entrain the niobium vapor. Clustering occurs inside a 5.7 cm long, 2 mm diameter tube such that a typical cluster undergoes $>10^5$ collisions. Thus any excess internal energy that may be present in the cluster from the vaporization process is dissipated.[15]

The resulting distribution of clusters and atoms expands into a vacuum chamber maintained at 180 mTorr. This mild supersonic expansion further cools internal and translational degrees of freedom.[16] The ions, gently focussed through three differentially pumped chambers, are accelerated in a region at 2×10^{-7} Torr for momentum analysis with a 60° sector magnet. With a mass range of 1 to 1000 amu, this momentum analyzer has sufficient resolution to pass ions of a single mass. The resulting continuous and mass-selected cluster ion beam is decelerated to a well-defined kinetic energy and then injected into an octopole ion beam guide.[17] The octopole passes through a reaction cell, where the ions interact with a neutral gas. To minimize multiple collision events, the Xe pressure is kept at ~0.1 mTorr (such that there is a 5% probability of a single collision for a cross section of 20 Å^2). Since reactions occur inside the ion beam guide, losses due to scattering are minimized, ensuring efficient product ion collection. After reaction, the transmitted ion beam and product ions are mass-analyzed by a quadrupole mass filter (5–1000 amu). Ion intensities are measured with standard pulse counting techniques. The end result is that the intensities of all reaction products are individually measured as a function of the interaction energy.

Ion intensities are converted to a total cross section via eq 1.[18] As

$$I_r = (I_r + \sum I_p) \exp(-\sigma_{tot} n_D l) \quad (1)$$

$$\sigma_p(E) = \sigma_{tot}(I_p/\sum I_p) \quad (2)$$

outlined previously,[17] raw background counts are subtracted from the foreground before cross sections are calculated. The subscripts r and p refer to the transmitted reactant and the pth product ion, n_D is the reactant gas number density, and l is the effective path length (8.3 cm). Individual product cross sections are calculated with eq 2.

The collision energy zero and ion energy distribution are determined by using the octopole ion guide as a retarding energy analyzer. The octopole is particularly effective as an energy analyzer because it practically eliminates low energy ion losses due to space charge effects. Additionally, the uncertainties associated with contact potentials and focussing aberrations are minimized because the retarding region is physically the same as the interaction region. The collision energy in the lab frame of an ion (of mass m) and a neutral reactant (of mass M) is converted to the center-of-mass (CM) frame with $E(CM) = E(lab)\text{-}M/(m + M)$. The absolute uncertainty in the energy scale is ±0.05 eV, lab frame.

Absolute cross section magnitudes have uncertainties of ±30%, mainly due to the gas cell length and pressure measurement. Relative cross section magnitudes have uncertainties of 5%, assuming efficient product collection. Product collection has previously been shown to be efficient for most CID processes of iron cluster ions.[15,19] Detection of low mass

(7) Walch, S. P.; Bauschlicher, C. W., Jr. In *Comparison of Ab Initio Quantum Chemistry with Experiment*; Bartlett, R. J., Ed.; D. Reidel: Dordrecht, 1985.
(8) Gupta, S. K.; Gingerich, K. A. *J. Chem. Phys.* **1979**, *70*, 5350.
(9) Gupta, S. K.; Gingerich, K. A. *J. Chem. Phys.* **1978**, *69*, 4318.
(10) Miedema, A. R.; Gingerich, K. A. *J. Phys. B* **1979**, *12*, 2081.
(11) Krasnov, K. S. *Teplofiz. Vys. Temp.* **1975**, *13*, 441.
(12) Cole, S. K.; Liu, K.; Riley, S. J. In *Physics of Chemistry of Small Clusters*; Jena, P., Rao, B. K., Khanna, S. N., Eds.; Plenum: New York, 1987.
(13) Cole, S. K.; Liu, K. *J. Chem. Phys.* **1988**, *89*, 780.
(14) Hanley, L.; Anderson, S. L. *Chem. Phys. Lett.* **1985**, *122*, 410.
(15) Loh, S. K.; Hales, D. A.; Lian, L.; Armentrout, P. B. *J. Chem. Phys.*, accepted for publication.
(16) Campargue, R. *J. Phys. Chem.* **1984**, *88*, 4466. Toennies, J. P.; Winkelmann, K. *J. Chem. Phys.* **1977**, *66*, 3965.
(17) Ervin, K. M.; Armentrout, P. B. *J. Chem. Phys.* **1985**, *83*, 166.
(18) Tatewaki, H.; Tomonari, M.; Nakamura, T. *J. Chem. Phys.* **1988**, *88*, 6419.
(19) Loh, S. K.; Lian, L.; Hales, D. A.; Armentrout, P. B. *J. Phys. Chem.* **1988**, *92*, 4009.

ions formed by dissociation of heavy clusters may not be as efficient, since these ions are not constrained to small laboratory scattering angles by conservation of momentum as severely as the heavier product ions are. Thus, the low mass product ions can have low-axial and high-transverse kinetic energies that cause them to be less efficiently transmitted through the quadrupole. This effect is clearly exacerbated at laboratory collision energies in excess of the DC bias of the quadrupole (−85 V). Below this energy, the lowest mass product ions (from the larger reactant cluster ions) may have cross sections with uncertainties as high as 50%, but these are reproducible to ±20%.

III. Dissociation Thresholds

In these experiments, the energy at which product formation begins (the cross section threshold) represents the barrier to dissociation. This in turn corresponds to the endothermicity of the process, if activation barriers are not present. This assumption has proven to be generally valid for ion–molecule reactions without barriers due to spin or orbit constraints.[20] Such barriers cannot be rigorously discussed, because the structures and electron configurations for the cluster electronic states are not known. In lieu of a more formal treatment, we can envision the dissociation process in reverse, where the products, Nb_p^+ and Nb_q, combine to form Nb_n^+. At long range, all potential surfaces are attractive because of the attractive ion-induced dipole potential. Let us assume that ground-state products, $Nb_p^+ + Nb_q$, correlate diabatically to a low-lying excited state of Nb_n^+ and that an excited-state dissociative asymptote leads to ground-state Nb_n^+. As Nb_q and Nb_p^+ approach, extensive mixing of these surfaces should occur, due to the fairly high densities of low-lying electronic states.[21] We anticipate that this mixing will result in avoided surface crossings, such that ground-state products correlate adiabatically to Nb_n^+ without barriers in excess of the dissociation energy. Thus, we assume that the observed threshold corresponds to the endothermicity of bond cleavage.

An apparent activation barrier can also be caused by a kinetic shift. Kinetic shifts can result from inefficient dissociation due to randomization of the available cluster internal energy into all internal modes, such as vibrational modes. This effect should become more pronounced for larger clusters that have more modes. In our experimental apparatus, dissociation must be sufficiently fast that it is complete during the time of flight of the ion from the point of collision (gas cell) to the quadrupole entrance, $\sim 1 \times 10^{-4}$ s.[15] Those collisionally energized clusters that do not dissociate within this time window will not be observed. If dissociation is slow compared to the experimental time scale, the threshold can be shifted to higher energies.

To evaluate this effect, we us RRKM theory to calculate the unimolecular rates of dissociation of these Nb clusters. To calculate $k(E)$, we must calculate the sum of states of the transition state at $E - E_0$ (the energy above the dissociation energy) and the density of states of the reactant cluster at E (the total energy).[22] These require the frequencies of the cluster vibrational modes. Since for niobium clusters these frequencies have yet to be measured or calculated for all but Nb_2, we use a method outlined by Jarrold and Bower (JB)[23] to obtain trial vibrational frequencies. The frequencies are extrapolated from the bulk using the Debye model of solid-state physics[24] and the Nb_2^+ frequency. Although the accuracy of these frequencies may not be absolutely correct, cancellation of errors occurs in division of the number of states by the density of states such that these calculations are at least a reasonable starting point for discussion. For Nb, the debye frequency is $\nu_D = 1200$ cm^{-1}.[25] The Nb_2^+ frequency is estimated as ~ 600 cm^{-1} from the calculated Nb_2 frequency of ~ 500 cm^{-1},[7] since the ion dimer BDE will be shown to be somewhat stronger than the neutral dimer BDE.

In addition, the reaction pathway degeneracy is assumed to equal n, the number of atoms in the cluster. This assumption is presumably good for small clusters where all atoms can be ejected from the cluster with nearly equal probability. Finally the numbers of states and the densities of states are calculated with Whitten–Rabinovich counting algorithms in the RRKM software developed by Hase and Bunker.[26]

It is found that dissociation of Nb_n^+ occurs faster than for Fe_n^+,[15] due to the relatively high vibrational frequencies of the Nb_n^+ clusters. The $k(E)$s rise sufficiently quickly with increasing energies above the thresholds that the dissociations should be complete on our experimental time scale. A kinetic shift, or inefficient product formation near the true threshold, is usually evident as a low-energy tail in the cross section. Such features are not observed in the present results. Further the RRKM calculations show that the dissociation rates for Nb_n^+ ($n \leq 5$) are sufficiently high that dissociation is prompt on our experimental time scale. Thus kinetic shifts do not appear to present a problem in the thresholds of these major product channels. The only exception is Nb_6^+ where the rate becomes slow enough to affect the threshold modestly. Our RRKM calculations indicate the Nb_6^+ thresholds can be shifted by as much as 0.10 ± 0.05 eV.

The cross sections may also be affected by product channel competition. In the event that dissociation of Nb_n^+ can yield two different product channels, the energy dependences of these cross sections can be influenced by each other. In some cases, one process may predominate so that the apparent threshold of the less probable process is not observed until higher energies. Such a situation may exist for product channels that have products that differ only by the location of the ionic charge. In these instances, relative IPs can be expected to affect product branching ratios. Care in the analysis is taken in these instances, as will be discussed below. Pointedly, the lowest energy dissociation pathway, usually $Nb_n^+ \rightarrow Nb_{n-1}^+ + Nb$, does not encounter competition until the energy exceeds the threshold of the next lowest energy process.

In a CID reaction, the endothermicity equals the sum of the cluster BDEs for the bonds that are broken. For example, if dissociation of Nb_n^+ occurs by loss of neutral atoms to form Nb_p^+, the threshold is given by eq 3. For fragmentation of Nb_n^+ and

$$E_0(\text{atomic}) = \sum_i^{n-p} D^\circ(Nb_{n-i}^+\text{–Nb}) \qquad (3)$$

Nb_q, some neutral cluster bonds remain unbroken. In these cases, the threshold represents the energy required to remove atoms from the cluster, E_0(atomic), minus the strength of the bonds in the molecular fragment(s) as given in eq 4. Thus, the BDEs of some

$$E_0(\text{molecular}) = E_0(\text{atomic}) - \sum_i^{q-1} D^\circ(Nb_i\text{–Nb}) \qquad (4)$$

smaller ionic and neutral fragments generally must be known to obtain information from the experimentally determined threshold. Equation 4 also shows that thresholds, in some instances, can furnish thermochemical information on the neutral clusters. If the neutral BDEs are already known, then the thresholds provide an internal check of the ionic cluster BDEs that are determined through CID of smaller clusters.

To obtain E_0, we use an empirical model to reproduce the threshold energy dependence of the cross section. It is assumed in this model that the threshold energy dependence reflects the energy dependence of the number of quantum states available for reaction rather than dynamic effects due to intermolecular forces. This assumption should be valid for dissociation processes and reactions of heavy particles that have large numbers of states available. The model is shown in eq 5. E and E_0 are the collision

$$\sigma_p(E) = \sigma_o(E - E_0)^N/E \qquad (5)$$

and threshold energies. σ_o is a scaling factor and N is an adjustable

(20) Gioumousis, G.; Stevenson, D. P. *J. Chem. Phys.* **1958**, *29*, 292.
(21) Loh, S. K.; Fisher, E. R.; Lian, L.; Schultz, R. H.; Armentrout, P. B. *J. Phys. Chem.*, accepted for publication.
(22) Theory summarized by: Robinson, P. J.; Holbrook, K. A. In *Unimolecular Reactions*; Wiley-Interscience: New York, 1972.
(23) Jarrold, M. F.; Bower, J. E. *J. Chem. Phys.* **1987**, *87*, 5728.
(24) Kittel, C. In *Introduction to Solid State Physics*; Wiley: New York, 1976; pp 136–9.
(25) Ashcroft, N. W.; Mermin, N. D. In *Solid State Physics*; Saunders College: Philadelphia, 1976; p 461.
(26) Code written by W. L. Hase and D. L. Bunker.

parameter. For comparison to the data, eq 5 is convoluted over the distributions of ion energy and thermal motion of the Xe.[17] Then the parameters N and E_0 are optimized to give the best linear least-squares fit to the data.

Past work has shown eq 5 to be sufficiently general to describe the threshold behaviors of numerous endothermic ion–molecule reaction cross sections and to provide accurate reaction thermochemistry.[27] This model has also been derived for and applied to diatom CID processes.[28-30] Models of this type have recently been applied to more complex cluster CID processes[31] and reactions[32] including CID of Fe_n^+.[15] Various values of N have been proposed, ranging from 1.5 to 2.5. Chesnavich and Bowers[33] have proposed a model based on transition-state theory where only translational energy is considered to contribute to the reaction coordinate. This treatment provides a general form of eq 5 that uses $N = 1.5$ for direct reactions of the type $Nb_n^+ \rightarrow Nb_{n-1} + Nb$ and $N = 2.5$ for $Nb_n^+ \rightarrow Nb_{n-2}^+ + Nb_2$.

IV. Results and Discussion

A. General Cross Section Features. The cross sections for CID of Nb_n^+ ($n = 2$–6) with Xe are shown in Figure 1. These clusters share several common cross section features. The total cross sections (the sum of the individual cross sections) rise smoothly and quickly from apparent thresholds of 4 to 6 eV. These are shown as solid lines. By 10 eV, the total cross sections slow their steep rise, leveling off to nearly constant values. In a CID process, bond cleavage can begin only when the collision energy exceeds the endothermicity. As discussed above, this exact energy threshold (E_0) is blurred experimentally by the distribution of collision energies. With increasing energies, collisions can impart more energy to the internal modes of a cluster, thereby increasing the probability for dissociation. As a result, the cross sections rise with increasing energy above threshold. But the dissociation probability cannot increase continually. Eventually at high energies, essentially all collisions transfer enough energy to the cluster to cause dissociation. Therefore, the total cross section for dissociation should become constant, representing a quasi-hard sphere cross section.

In fact, the total cross sections attain nearly constant values at energies above 15 eV. That the total cross sections are constant and do not decrease with increasing energy attests to the efficiency of the product ion collection. The magnitudes of the cross sections at these high energies increase monotonically from the dimer, 4 Å^2, to a maximum at the hexamer of 20 Å^2, as qualitatively expected in a hard sphere model for clusters of increasing size.

The lowest energy pathway for dissociation of Nb_n^+ is found to be formation of Nb_{n-1}^+, or loss of a single Nb atom from the cluster. This ionic product is the dominant dissociation product throughout the entire enerty range that is examined in this study, 0 to 25 eV. Nb_4^+ presents the lone exception. In CID of Nb_4^+, formation of Nb_2^+ is found to have the lowest threshold energy, although Nb_3^+ formation becomes energetically accessible soon after and is the dominant product at higher energies. With CID of each cluster, all possible ionic products are observed with increasing collision energies. The fall-off above 85 eV (lab) observed for the smallest products (obvious in Figure 1, d and e) is almost certainly due to poor transmission of these ions through the quadrupole, as discussed above.

Nb_2^+. CID of Nb_2^+ has only one product channel, $Nb^+ + Nb$. Analysis of the energy dependence of the cross section threshold is accomplished with eq 5. The best fit of the data from 5 to 11 eV is given by $N = 1.65 \pm 0.10$ and $E_0 = 6.15 \pm 0.15$ eV. The parameters used in the analysis of each cross section threshold are given in Table I. The analysis of the $Nb_2^+ \rightarrow Nb^+ + Nb$ cross section energy dependence is shown in Figure 2, where the data are plotted on a linear cross section and expanded energy axes. As shown, this form of the model provides an excellent reproduction of the data down to the noise level. The uncertainties in all reported E_0s arise from closely related forms of the model that adequately fit the data and the absolute uncertainty in the energy scale (0.05 eV lab). As discussed above, we expect that E_0 corresponds directly to the bond dissociation energy. Thus, we measure $D°(Nb_2^+) = 6.15 \pm 0.15$ eV.

Table I. Nb_n^+ CID Cross Section Analyses[a]

size n		$\sigma(Nb_{n-x}^+-Nb_x)$ $x = 1$	$x = 2$	$x = 3$	$x = 4$	$x = 5$
2	E_0	6.15 (0.15)				
	N	1.65 (0.10)				
3	E_0	4.60 (0.15)	5.64 (0.20)			
	N	1.75 (0.10)	2.10 (0.15)			
4	E_0	5.90 (0.20)	5.16 (0.20)	7.0 (0.6)		
	N	2.40 (0.15)	1.90 (0.15)	1.5 (0.5)		
5	E_0	5.50 (0.20)	6.40 (0.25)	7.8 (0.3)	8.5 (0.5)	
	N	1.90 (0.15)	2.30 (0.15)	1.65 (0.15)	*b*	
6	E_0	5.65 (0.20)	5.85 (0.20)	8.7 (0.4)	8.7 (0.4)	~9 (0.4)
	N	2.00 (0.15)	2.50 (0.15)	*b*	*b*	*b*

[a] Cross section thresholds (E_0s) given in eV. N is a parameter in the empirical model given by eq 5 in the text. [b] From visual inspection.

Nb_3^+. In this system, two ionic products are possible and observed (Figure 1b). Dissociation of Nb_3^+ to $Nb_2^+ + Nb$ is observed to be the dominant process throughout the energy range. Analysis of this cross section, as given in Table I, provides $D°(Nb_2^+-Nb) = 4.60 \pm 0.15$ eV. The model used, shown in Figure 3, yields an excellent reproduction of the data to the lowest energies.

The formation of Nb^+ can proceed via two product channels, $Nb^+ + Nb_2$ or $Nb^+ + 2Nb$. The former should become energetically accessible at an energy lower than the latter by $D°(Nb_2)$. Therefore, these two processes should be easily distinguished by their thresholds. Production of $Nb^+ + 2Nb$, requiring complete atomization of the cluster, must have a threshold equal to the sum of the bonds in the cluster, $E_0(Nb^+ + 2Nb) = D°(Nb_2^+-Nb) + D°(Nb^+-Nb)$, as noted in eq 3. Since these BDEs are derived above, $E_0(Nb^+ + 2Nb) = 4.60\ (\pm 0.15) + 6.15\ (\pm 0.15) = 10.75\ (\pm 0.21)$ eV. This result is clearly at odds with the apparent threshold of ~6 eV (Figure 1b). Therefore, formation of Nb^+ near threshold must correspond to neutral dimer formation, $Nb_3^+ \rightarrow Nb^+ + Nb_2$.

To obtain a quantitative E_0 for this process, $\sigma(Nb^+)$ is modeled with eq 5 and the parameters listed in Table I. The analysis is shown in Figure 3. The significantly higher value of $N = 2.1$ required to model $\sigma(Nb^+ + Nb_2)$ reflects its slower rise from threshold than the primary process, $\sigma(Nb_2^+ + Nb)$, where $N = 1.75$. These behaviors are probably indicative of competition between the $Nb_3^+ \rightarrow Nb_2^+ + Nb$ and $Nb_3^+ \rightarrow Nb_2 + Nb^+$ product channels. This is not unexpected, since the product channels differ only by the final location of the charge. As a result, the difference in threshold energies of these processes ($\Delta E_0 = 1.04 \pm 0.25$ eV) represents the difference in IPs presented in eq 6a. These product

$$E_0(Nb^+ + Nb_2) - E_0(Nb_2^+ + Nb) = IP(Nb) - IP(Nb_2) \quad (6a)$$

$$= D°(Nb_2^+) - D°(Nb_2) \quad (6b)$$

channels also differ by the bond energies of the dimers, as shown in eq 6b, allowing determination of the neutral dimer BDE. Substituting in the required values from Table I into relation 6b gives $D°(Nb_2) = 5.11 \pm 0.29$ eV, snugly within the broad uncertainties of the previous value of 5.0 ± 0.4 eV.

Nb_4^+. The cross sections for $Nb_4^+ + Xe$ are shown in Figure 1c. These have been compared with the CID cross sections of Fe_4^+ in a recent publication.[34] Nb_4^+ is the only cluster for which

(27) Aristov, N.; Armentrout, P. B. *J. Am. Chem. Soc.* **1986**, *108*, 1806. Boo, B. H.; Armentrout, P. B. *J. Am. Chem. Soc.* **1987**, *109*, 3549. Sunderlin, L.; Aristov, N.; Armentrout, P. B. *J. Am. Chem. Soc.* **1987**, *109*, 78. Elkind, J. L.; Armentrout, P. B. *J. Phys. Chem.* **1987**, *91*, 2037.
(28) Maier, W. B., II *J. Chem. Phys.* **1964**, *41*, 2174.
(29) Levine, R. D.; Bernstein, R. B. *Chem. Phys. Lett.* **1971**, *11*, 552.
(30) Parks, E. K.; Hansen, N. J.; Wexler, S. *J. Chem. Phys.* **1973**, *58*, 5489. Parks, E. K.; Wagner, A.; Wexler, S. *J. Chem. Phys.* **1973**, *58*, 5502. Parks, E. K.; Kuhry, J. G.; Wexler, S. *J. Chem. Phys.* **1977**, *67*, 3014.
(31) Hanley, L.; Ruatta, S. A.; Anderson, S. L. *J. Chem. Phys.* **1987**, *87*, 260.
(32) Jarrold, M. F.; Bower, J. E. *J. Am. Chem. Soc.* **1988**, *110*, 70.
(33) Chesnavich, W. J.; Bowers, M. T. *J. Phys. Chem.* **1979**, *83*, 900.

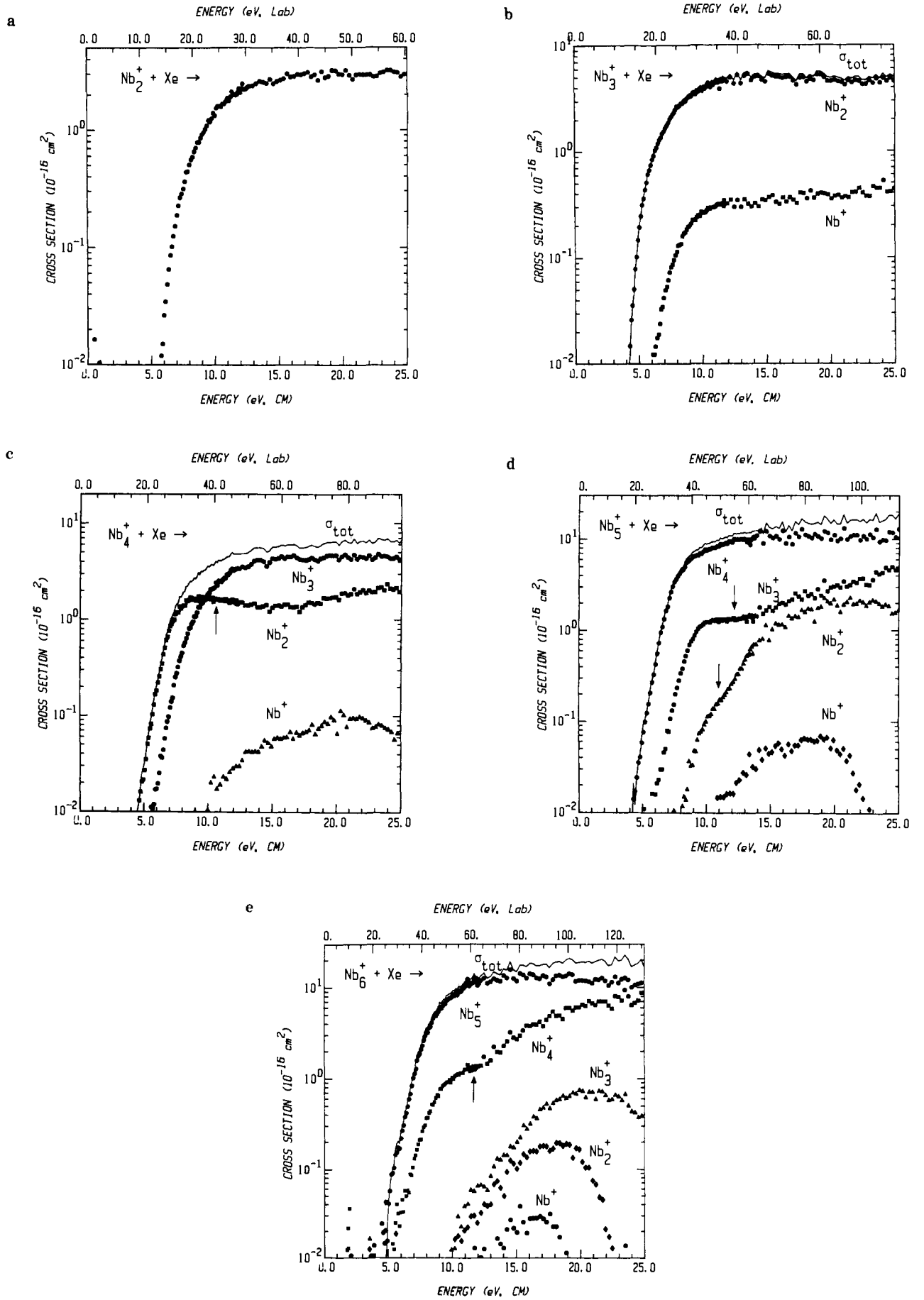

Figure 1. Collision-induced dissociation of niobium cluster ions, $Nb_n^+ + Xe$, $n = 2$–6, parts a–e. The CID cross sections, measured in Å^2, are plotted as functions of collision energy in the center-of-mass (lower x-axis) and laboratory (upper x-axis) frames. Total cross sections for dissociation are shown as solid lines. Arrows indicate thresholds for higher energy processes that produce fragment ions, discussed in the text.

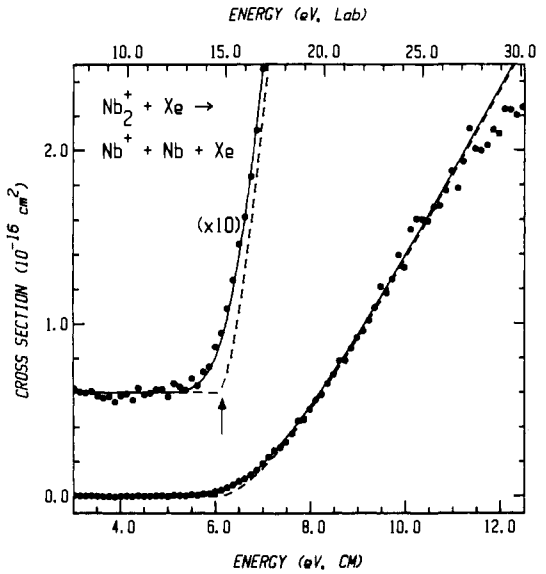

Figure 2. Analysis of the cross section energy dependences of Nb_2^+ + Xe → Nb^+ + Nb + Xe. The cross section is plotted as a function of collision energy in the center-of-mass (lower x-axis) and laboratory (upper x-axis) frames. An empirical model, discussed in the text, and the model convoluted with the experimental energy distributions are indicated by dashed and solid lines, respectively. E_0 is denoted by an arrow.

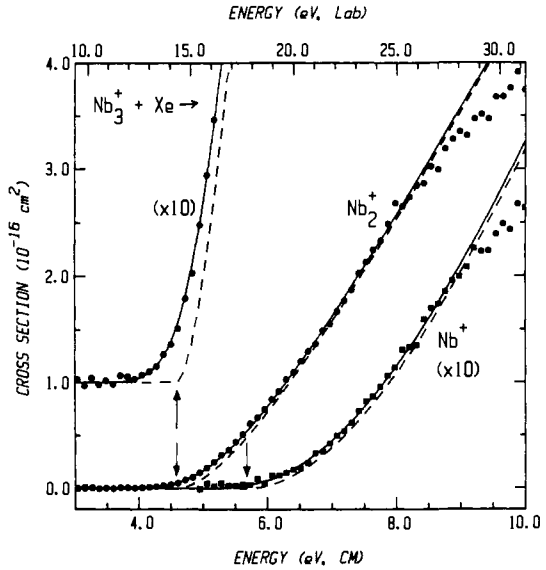

Figure 3. Analysis of the cross section energy dependences of Nb_3^+ + Xe. The cross sections are plotted as a function of collision energy in the center-of-mass (lower x-axis) and laboratory (upper x-axis) frames. An empirical model and the model convoluted with the experimental energy distributions are indicated by dashed and solid lines, respectively. E_0s are denoted by arrows.

Nb_{n-1}^+ is not the lowest energy ionic product, demonstrating rather dramatically that Nb_2^+ must be accompanied by Nb_2 formation near threshold. $\sigma(Nb_2^+)$ is observed to be larger than $\sigma(Nb_3^+)$ from its threshold to ~9 eV, at which the probabilities of Nb_2^+ and Nb_3^+ production become equal. At higher energies, Nb_3^+ becomes the dominant product. Nb^+ remains a relatively minor product throughout the energy range examined.

Analyses of $\sigma(Nb_2^+ + Nb_2)$ and $\sigma(Nb_3^+ + Nb)$ are given in Table I and shown in Figure 4. Again the value of N is higher for the higher energy process, Nb_3^+ + Nb, than for the lowest energy process, Nb_2^+ + Nb_2. This again implies competition between these channels, although now this competition is not as simple

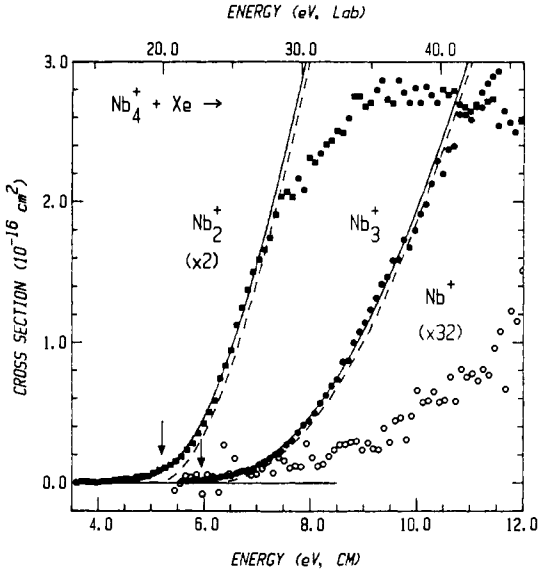

Figure 4. Analysis of the cross section energy dependences of Nb_4^+ + Xe. The cross sections are plotted as a function of collision energy in the center-of-mass (lower x-axis) and laboratory (upper x-axis) frames. An empirical model and the model convoluted with the experimental energy distributions are indicated by dashed and solid lines, respectively. E_0s are denoted by arrows.

as the location of charge. The threshold energies are found to differ by 0.74 ± 0.28 eV, which is the energy required to break the Nb_2^+–Nb bond less the energy that is gained by forming a Nb–Nb bond, eq 7. This comparison of *relative* thresholds implies

$$E_0(Nb_3^+ + Nb) - E_0(Nb_2^+ + Nb_2) = D°(Nb_2) - D°(Nb_2^+ - Nb) \quad (7)$$

that $D°(Nb_2) = 5.34 \pm 0.32$ eV, in reasonable agreement with the value of 5.11 ± 0.29 eV obtained from analysis of the Nb_3^+ system.

A new channel for Nb_2^+ production is observed as an increase in the Nb_2^+ cross section at about 15 eV (Figure 1c). Since the total cross section is relatively constant (indicating that the total product ion intensity is constant), the additional Nb_2^+ intensity must result from decomposition of the Nb_3^+ product, such that $Nb_4^+ \rightarrow Nb_2^+ + 2Nb$ takes place at high energy. The threshold is not obvious until ~4 eV higher than its calculated value of 10.50 ± 0.28 eV, presumably due to the dominance of the $Nb_2^+ + Nb_2$ process which obscures the threshold of this minor product channel.

Nb^+ formation has a very low probability such that the cross section is near our sensitivity limit. Analysis of the threshold (Table I) gives $E_0(Nb^+) = 7.0 \pm 0.6$ eV, where the large uncertainty reflects the scatter in the data. The threshold energies for the $Nb^+ + 3Nb$ and $Nb^+ + Nb_2 + Nb$ product channels [calculated with $D°(Nb_2) = 5.19 \pm 0.28$ eV, as discussed below] are 16.7 ± 0.3 and 11.5 ± 0.4 eV, respectively, showing that $Nb_4^+ \rightarrow Nb^+ + Nb_3$ must be the dominant process near threshold. In this case, the differences in the thresholds for the various product channels again can be related to IPs and cluster BDEs, eq 8a and 8b. IP(Nb_3), which will be discussed in a later section, can be

$$E_0(Nb^+ + Nb_3) - E_0(Nb_3^+ + Nb) = IP(Nb) - IP(Nb_3) \quad (8a)$$

$$E_0(Nb^+ + Nb_3) - E_0(Nb_2^+ + Nb_2) = D°(Nb^+ - Nb) - D°(Nb_2 - Nb) \quad (8b)$$

obtained from the relative thresholds for Nb^+ and Nb_3^+ formation, via eq 8a. Equation 8b allows the Nb_3 BDE to be derived from the Nb_2^+ BDE. We find $D°(Nb_2 - Nb) = 4.3 \pm 0.7$ eV, indicating that the neutral trimer is probably bound somewhat more weakly than the trimer ion.

Nb_5^+. Again, all possible ionic products are observed to be formed in the CID of Nb_5^+ (Figure 1d). Analysis of the two lowest energy processes, $\sigma(Nb_4^+)$ and $\sigma(Nb_3^+)$, yields $E_0(Nb_4^+) = D°(Nb_4^+ - Nb) = 5.50 \pm 0.20$ eV and $E_0(Nb_3^+) = 6.40 \pm 0.25$

(34) Loh, S. K.; Lian, L.; Hales, D. A.; Armentrout, P. B. *J. Chem. Phys.* **1988**, *89*, 610.

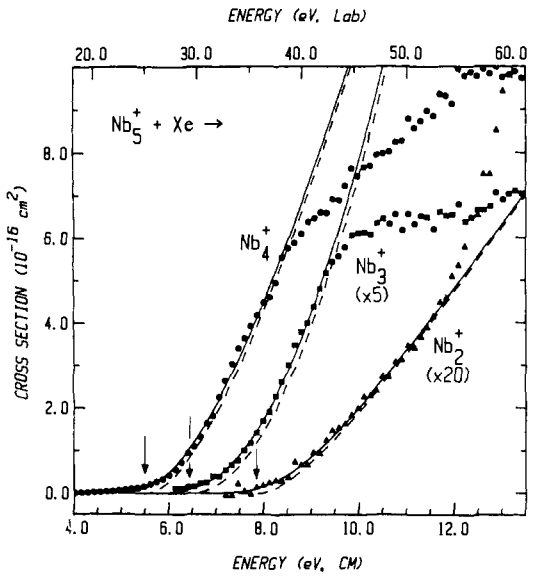

Figure 5. Analysis of the cross section energy dependences of Nb_5^+ + Xe. The cross sections are plotted as a function of collision energy in the center-of-mass (lower x-axis) and laboratory (upper x-axis) frames. An empirical model and the model convoluted with the experimental energy distributions are indicated by dashed and solid lines, respectively. E_0s are denoted by arrows.

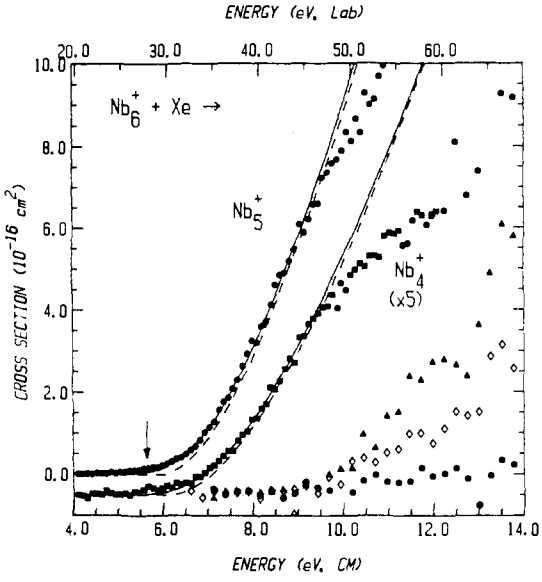

Figure 6. Analysis of the cross section energy dependences of Nb_6^+ + Xe. The cross sections are plotted as a function of collision energy in the center-of-mass (lower x-axis) and laboratory (upper x-axis) frames. An empirical model, and the model convoluted with the experimental energy distributions are indicated by dashed and solid lines, respectively. The E_0 for the lowest energy process is denoted by an arrow. The Nb_3^+ (solid triangles), Nb_2^+ (open diamonds), and Nb^+ (solid circles) cross sections are shown expanded by a factor of 50.

eV, as seen in Table I and Figure 5. These analyses show that $\sigma(Nb_3^+)$ rises more slowly from threshold (with a higher N value) than does $\sigma(Nb_4^+)$. The difference in thresholds is determined to be 0.90 ± 0.32 eV, in this instance corresponding to $D°(Nb_3^+–Nb) - D°(Nb_2)$. Thus, the relative thresholds give another value of the neutral dimer BDE, $D°(Nb_2)$ = 5.00 ± 0.38 eV.

The energy dependence of Nb_3^+ formation is similar to that of Nb_2^+ observed in CID of Nb_4^+. The cross section has a noticeable rise beginning at ~12 eV (Figure 1d) due to additional intensity from decomposition of a larger product ion. In this case, it is decomposition of the Nb_4^+ product to Nb_3^+, which results in the overall process $Nb_5^+ \rightarrow Nb_3^+ + 2Nb$. In good agreement, the threshold for this process should be 5.50 (±0.20) + 5.90 (±0.20) = 11.40 ± 0.28 eV.

The cross section for Nb_2^+ formation also has an unusual shape, with apparently two contributing processes. This is clearly shown in Figure 5, where the first feature rises nearly linearly from threshold and a second feature appears as an increase in the cross section at ~11 eV. Similarly, we assign this feature to Nb_2^+ intensity from decomposition of a larger ionic product. The first feature is best modeled with N = 1.65 ± 0.15 and E_0 = 7.8 ± 0.3 eV, a different threshold behavior than noted in similar processes observed in the CID systems above. A sharper rise from threshold is observed here, probably due to dynamic effects.

Still, we can determine the low energy product channel by its threshold. The thresholds calculated for the three possible Nb_2^+ product channels, assuming the values $D°(Nb_2–Nb)$ = 4.3 ± 0.7 and $D°(Nb–Nb)$ = 5.19 ± 0.28 eV (which will be derived from consideration of all the systems, see below), are listed in eq 9a–c.

$$Nb_5^+ \rightarrow Nb_2^+ + Nb_3 \ (-6.5 \pm 0.8 \text{ eV}) \quad (9a)$$

$$\rightarrow Nb_2^+ + Nb_2 + Nb \ (-10.8 \pm 0.4 \text{ eV}) \quad (9b)$$

$$\rightarrow Nb_2^+ + 3Nb \ (-16.0 \pm 0.3 \text{ eV}) \quad (9c)$$

The threshold of 7.8 eV is considerably less than those of reaction 9b or 9c, hence Nb_2^+ must be accompanied by Nb_3 formation, reaction 9a. By using $E_0(Nb_2^+)$ = 7.8 ± 0.3 eV and eq 4, the $Nb_2–Nb$ BDE is estimated as 3.0 ± 0.5 eV, which is somewhat lower than $D°(Nb_2–Nb)$ = 4.3 ± 0.7 eV derived in the tetramer system. However, the contrast in the energy dependence of this cross section (with respect to those of similar processes in the other systems) implies that dynamic effects or a kinetic shift may be influencing the shape of the cross section. Due to such effects, Nb_2^+ production may not be observed at threshold. As a result, the threshold from this analysis represents a lower limit to the BDE, $D°(Nb_2–Nb) \geq 3.0 \pm 0.5$ eV. Note, however, that the relative E_0s of Nb_3^+ and Nb_2^+ clearly imply that $IP(Nb_3) < IP(Nb_2)$.

A second product channel for Nb_2^+ formation becomes energetically accessible at ~11 eV, where the data rise faster than the threshold model (Figure 5). This energy agrees nicely with the energetics of $Nb_2^+ + Nb_2 + Nb$ formation (reaction 9b). The mechanism for this process can be procured from relative cross section behaviors. One way that $Nb_2^+ + Nb_2 + Nb$ could be formed is through dissociation of $Nb_2^+ + Nb_3$, but this process does not create additional Nb_2^+ intensity. Instead, a higher order product, such as Nb_4^+ or Nb_3^+, must dissociate. Decomposition of Nb_3^+ should appear as a decrease in $\sigma(Nb_3^+)$ at 11 eV, since it is a relatively small cross section. Instead, this cross section increases near 11 eV. As a result, Nb_3^+ decomposition appears not to be the cause of added Nb_2^+ intensity. Recalling the Nb_4^+ CID system examined above, we see that Nb_4^+ fragments to Nb_2^+ and to Nb_3^+ by ~6 eV. Turning back to the Nb_5^+ system, we note that the new channels for Nb_2^+ and Nb_3^+ formation appear to open at ~6 eV above the E_0 for $Nb_5^+ \rightarrow Nb_4^+ + Nb$ and they have the qualitative proportions expected from the Nb_4^+ CID system. Therefore the increases in these two cross sections must be due to Nb_4^+ decomposition. The net processes can be written as $Nb_5^+ \rightarrow Nb_2^+ + Nb_2 + Nb$ and $Nb_5^+ \rightarrow Nb_3^+ + 2Nb$.

The Nb^+ product cross section is too small for threshold analysis with eq 5, but from visual inspection, the apparent threshold is 8.5 ± 0.5 eV. This value (along with eq 4) implies that $D°(Nb_3–Nb) \geq 4.2 \pm 0.8$ eV. This is a lower limit due to the possibility of competing processes and our experimental sensitivity limits.

Nb_6^+. The cross sections for CID of Nb_6^+ are shown in Figure 1e. $Nb_5^+ + Nb$ is the dominant product channel at low energies, but it is apparent that $Nb_4^+ + Nb_2$ is also formed at fairly low energies. The Nb_4^+ cross section rises smoothly and quickly from threshold and begins to level out at ~9 eV. A sudden increase is observed at 12 eV, due to decomposition of Nb_5^+ to $Nb_4^+ + Nb$, a process that becomes energetically accessible at 11.2 ± 0.3 eV.

Analysis of the two lowest energy processes is shown in Figure 6 and the parameters are given in Table I. As previously mentioned, this is the only system where dissociation appears not to

Table II. Summary of Thermodynamic Information (eV)[a]

n	$D°(Nb_{n-1}^+–Nb)$	$D°(Nb_{n-1}–Nb)$	$IP(Nb_n)$
1			6.88 (0.0001)[b]
2	6.15 (0.15)	5.19 (0.28)	5.92 (0.32)
3	4.60 (0.15)	4.3 (0.7)	5.6 (0.8)[c]
4	5.90 (0.20)	5.9 (0.8)[d]	5.58 (0.05)[e]
5	5.50 (0.20)	5.35 (0.21)[d]	5.43 (0.05)[e]
6	5.65 (0.20)[f]	5.54 (0.21)[d]	5.34 (0.05)[e]

[a] All values derived from this work except as noted. Uncertainties given in parentheses. [b] Reference 38. [c] Also, $IP(Nb_3) < IP(Nb_2)$ from branching ratios and relative thresholds, see text. [d] Derived from ionic bond dissociation energies and ionization potentials as in eq 11. [e] Reference 37. [f] Includes a 0.10 ± 0.05 shift from the RRKM model discussed in the text.

occur efficiently at energies just above threshold. To account for this effect, threshold analyses are performed with the RRKM considerations outlined above. The result is that the E_0s for both processes include an RRKM shift of 0.10 ± 0.05 eV. The difference in the Nb_4^+ and Nb_5^+ thresholds of 0.20 ± 0.28 eV gives another measure of the Nb_2 BDE. By solving eq 4, formulated for this system, $D°(Nb_2) = D°(Nb_4^+–Nb) - 0.20$ (±0.28) = 5.30 ± 0.35 eV, providing reasonable agreement with the values obtained from the other systems.

The Nb_3^+ and Nb_2^+ products have small cross sections. These are shown in Figure 6, without analysis. These two cross sections have apparent thresholds that are indistinguishable at 8.7 ± 0.4 eV. The expected thresholds for the product channels that form the largest molecular neutral product possible, derived with eq 4, are shown in reactions 10a and 10b. These equations assume

$$Nb_6^+ \rightarrow Nb_3^+ + Nb_3 \ (-7.6\ (\pm 0.8)\ eV) \qquad (10a)$$

$$\rightarrow Nb_2^+ + Nb_4 \ (-12.2\ (\pm 0.8)\ eV + D°(Nb_3–Nb)) \qquad (10b)$$

$D°(Nb–Nb) = 5.19 \pm 0.28$ eV and $D°(Nb_2–Nb) = 4.3 \pm 0.7$ eV, as derived from consideration of all the systems, see below. As can be seen, reactions 10a and 10b must be the respective processes that occur near the thresholds, since other processes have thresholds that are higher by approximately 5 eV. Instead of assuming a value of $D°(Nb_3)$, we can use reaction 10a, $D°(Nb_2) = 5.19 \pm 0.28$ eV derived below, and the observed threshold of $\sigma(Nb_3^+)$ to determine $D°(Nb_2–Nb) = 3.2 \pm 0.6$ eV. This represents a lower limit, since the product intensities are close to the instrumental sensitivity limits. We can also use relations 10a and 10b (or equivalently, eq 4) and the apparent equivalence of $E_0(Nb_3^+)$ and $E_0(Nb_2^+)$ to infer that $D°(Nb_3–Nb) \simeq D°(Nb_2^+–Nb)$. Because competition with $Nb_2 + Nb_4^+$ production can raise the threshold for $Nb_2^+ + Nb_4$ formation, while symmetrical Nb_6^+ cleavage to $Nb_3^+ + Nb_3$ has no directly competitive processes, this equality is probably a limit, $D°(Nb_3–Nb) \geq D°(Nb_2^+–Nb) = 4.60 \pm 0.15$ eV.

Formation of Nb^+ has an apparent threshold of ~9 eV, as seen in Figure 6. Since the $IP(Nb_5)$ has been measured previously (Table II), the thermodynamic threshold for formation of $Nb^+ + Nb_5$ is higher than that for $Nb_5^+ + Nb$ formation by 1.45 ± 0.05 eV, namely at 7.1 ± 0.2 eV. Since other processes that form Nb^+ have thresholds that are higher by more than 5 eV, the low-energy process must be formation of the intact Nb_5 neutral. The apparent threshold is presumably much higher than the thermodynamic threshold because the cross section is near our sensitivity limits and because competition with other more favorable channels can affect the cross section.

B. Summary of Thermochemical Information. The ionic BDEs of Nb_n^+ (n = 2–6) are derived directly from threshold analyses and are summarized in Table II. However, it is from relative threshold measurements that the neutral Nb_n BDEs are derived. As we have noted, $\sigma(Nb_{n-1}^+)$ are best modeled with forms of eq 5 that use $N \simeq 1.7$, whereas $\sigma(N_{n-2}^+)$, require $N \simeq 2.3$ (Table I). Such values of N are actually fairly well predicted by the theory of Chesnavich and Bowers for reactions of this type.[33] This difference in N is significant because it shows that $\sigma(Nb_{n-1}^+)$ rise more quickly from threshold than do $\sigma(Nb_{n-2}^+)$. However, the exact opposite behaviors are observed in the Nb_4^+ system. This is indicated in Table I for n = 4, where the modeling of $\sigma(Nb_{n-1}^+)$ requires a higher value of N than does $\sigma(Nb_{n-2}^+)$. Coincidentally, the Nb_4^+ CID system is the only system for which the $\sigma(Nb_{n-2}^+)$ channel has a lower threshold than $\sigma(Nb_{n-1}^+)$.

These observations suggest that, in each system, the cross section with the lowest threshold energy rises more quickly (i.e. requires a lower value of N) than does a cross section with a higher threshold. The reason for this behavior is probably competition between the various reaction channels. The low-energy process, which has no competition at threshold, rises fairly sharply from threshold. In contrast, the second process, which must compete with the ongoing primary process at all energies above its threshold, therefore rises more slowly from threshold.

As discussed above, the threshold measurements in four separate CID systems yield four values of $D°(Nb_2)$: 5.11 ± 0.29, 5.34 ± 0.32, 5.00 ± 0.38 eV, and 5.30 ± 0.35 eV. These result from comparison of the relative thresholds of $Nb_n^+ \rightarrow Nb_{n-1}^+ + Nb$ and $Nb_n^+ \rightarrow Nb_{n-2}^+ + Nb_2$ (n = 3–6). Averaging these values, we obtain $D°(Nb_2) = 5.19 \pm 0.28$ eV, where the uncertainty derived is from the pooled estimate of error.[35] Our value also agrees nicely with the limits obtained by including the BDEs obtained from theoretical studies, $D°(Nb_2) = 5.0 \pm 0.4$ eV. It also is in good agreement with the Knudsen cell results,[8] where the second and third law treatments give 5.57 ± 0.41 and 5.22 ± 0.02 eV, respectively. It does not agree with the reevaluated third law value of 4.86 ± 0.02 eV.[2]

The neutral trimer and tetramer BDEs can also be derived from these studies. From the Nb_4^+ system, the trimer BDE is determined to be 4.3 ± 0.7 eV, which agrees with the limits derived in the pentamer and hexamer systems of >3.0 ± 0.5 and >3.2 ± 0.6 eV, respectively. As a result, we report $D°(Nb_2–Nb) = 4.3 \pm 0.7$ eV. The neutral tetramer BDE is bracketed by Nb^+ and Nb_2^+ threshold analyses in the Nb_5^+ and Nb_6^+ systems, respectively. These show that $D°(Nb_3–Nb) > 4.2 \pm 0.8$ eV and $> 4.6 \pm 0.15$ eV.

The neutral and ionic BDEs allow the IPs of these clusters to be determined. The generalized relation is shown in eq 11. From

$$IP(Nb_n) = IP(Nb_{n-1}) - D°(Nb_{n-1}^+–Nb) + D°(Nb_{n-1}–Nb) \qquad (11)$$

the final bond energies listed in Table II, Nb_2^+ is found to be more strongly bound than Nb_2 by 0.96 ± 0.32 eV. This is in good agreement with the value (1.04 ± 0.25 eV) that we obtain directly from the threshold difference of the $Nb_3^+ \rightarrow Nb_2^+ + Nb$ and $Nb_3^+ \rightarrow Nb_2 + Nb^+$ reactions. From the literature value of IP(Nb) = 6.883 ± 0.0001 eV and our BDE determinations, we obtain $IP(Nb_2) = 5.92 \pm 0.32$ eV. With this value and the neutral and ionic trimer BDEs given in Table II, eq 11 yields $IP(Nb_3) = 5.6 \pm 0.8$ eV. Note that $IP(Nb_2) > IP(Nb_3)$, in agreement with the branching ratio observed for Nb_5^+ decomposing to Nb_3^+ and Nb_2^+. Neither the IP of Nb_2 nor that of Nb_3 have been measured previously; however, niobium clusters, in contrast to atomic Nb, are found to be single-photon ionized by an ArF laser.[36] These results imply that $IP(Nb_n) < 6.42$ eV.

The IPs of larger clusters are known[37] and those within the range of this study are listed in Table II. We can use $IP(Nb_3)$, $D°(Nb_4^+)$, and the known $IP(Nb_4)$ to obtain a neutral tetramer BDE, by again solving eq 11. The result is $D°(Nb_3–Nb) = 5.9 \pm 0.8$ eV which agrees with our lower limit of 4.60 ± 0.15 eV. The IPs of Nb_n (n = 4–6) can be used in conjunction with our ionic BDEs to calculate $D°(Nb_5) = 5.35 \pm 0.21$ and $D°(Nb_6) = 5.54 \pm 0.21$ eV.

C. Size-Dependent Trends. In Figure 7, the ionic niobium cluster BDEs derived in this work are shown graphically. Within this range of cluster sizes, the $Nb^+–Nb$ bond is the strongest,

(35) Box, G. E. P.; Hunter, W. G.; Hunter, J. S. In *Statistics for Experimenters*; Wiley: New York, 1978; p 319.
(36) Prof. M. D. Morse (private conversations).
(37) Cox, D. M.; Whetten, R. L.; Zakin, M. R.; Trevor, D. J.; Reichmann, K. C.; Kaldor, A. *Proc. Int. Laser Sci. Conf.* **1986**, 527. Whetten, R. L.; Zakin, M. R.; Cox, D. M.; Trevor, D. J.; Kaldor, A. *J. Chem. Phys.* **1986**, *85*, 1697.

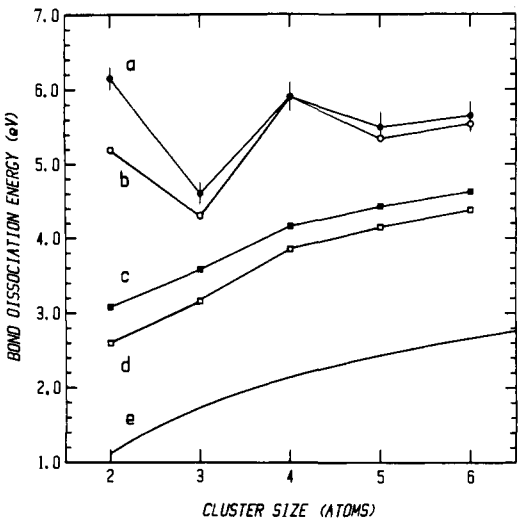

Figure 7. $D°(Nb_{n-1}^+-Nb)$ (closed circles labeled a, including error bars) and $D°(Nb_{n-1}-Nb)$ (open circles labeled b) derived in this work plotted as a function of cluster size. The dissociation energy per atom of the ionic and neutral Nb clusters (closed squares labeled c and open squares labeled d, respectively) is plotted. Also shown is an empirical form[39] (line labeled e) intended to model the convergence of the binding energy per atom of metal clusters to ΔH_{sub} (Nb,s) with increasing cluster size.

whereas the Nb_2^+–Nb bond is the weakest. An odd–even variation in bond strength is noted, although the size range of this study is fairly short. Also shown are the binding energies per cluster atom. With larger cluster sizes, this quantity must eventually converge to the heat of sublimation of Nb(s), 7.59 ± 0.08 eV.[38] A steady rise is observed toward this limit.

The convergence of the per atom binding energy to ΔH_{sub} has been modeled previously.[39] An empirical model was proposed based on experimental data from the homogeneous condensation of supersaturated Fe vapor (to Fe_n, $n = 10^2$ to 5×10^3 atoms) and from previous calculations on small clusters of a variety of metals. This form is given by eq 12. E_0(atomic) is the energy

$$E_0(\text{atomic})/n = \Delta H_{sub}(1 - n^{-0.25}) \qquad (12)$$

required for complete atomization of the cluster, calculated by eq 3. While this formula reproduces our experimental data for small iron clusters remarkably well, Figure 7 shows that it does not reproduce our niobium cluster data. Hence, eq 12 does not appear to be universal. However, similar empirical forms may allow the binding energies of larger Nb clusters to be extrapolated from data on smaller species.

Also shown in Figure 7 are the neutral cluster BDEs. These show a similar size dependence as the ionic clusters. The largest difference in ionic and neutral binding energies is found between the dimers. With increasing size, the neutral and ionic BDEs become nearly equal, although the ions are consistently more strongly bound than their neutral counterparts by about 0.1 eV. This is probably due to extra stabilization from the ion-induced dipole attraction.[40]

The ionization potentials of the clusters examined here decline monotonically with size. When compared with values for vanadium clusters measured by photoionization where $IP(V_3) < IP(V_4) < IP(V_2) < IP(V)$,[37] our values all seem reasonable although our trimer IP may be somewhat high. While this comparison is not definitive, it does suggest that the IP values for the dimer and trimer clusters are accurate within the generous uncertainty limits cited.

Our results indicate that the niobium cluster bond strengths are considerably higher than those found by Brucat et al., where $D°(Nb_{n-1}^+-Nb) < 2.33$ eV for $n = 3$–10.[5] The obvious explanation for the discrepancy is that the photofragmentation observed was a result of multiphoton processes, which would give bond energies that are anomalously low. As pointed out by a referee, however, except for Nb_3^+, our bond energy values for Nb_n^+ ($n = 4$–6) imply that *three* 2.33-eV photons are required for photodissociation. While this seems improbable, there are several reasons why we believe this is the most likely explanation. First, the fluence dependence measurements necessary to establish the number of photons needed for photofragmentation are notoriously difficult. Second, it is even more improbable that the CID thresholds are shifted up by over 3 eV from a thermodynamic value of <2.3 eV (although a shift up from a two-photon threshold of <4.66 eV may be plausible). Third, there seems little reason to doubt our bond energy for Nb_2^+ and Nb_3^+ since they lead to reasonable values for the neutral bond energies and ionization potentials. Thus, the high bond strengths of the tetramer, pentamer, and hexamer ions are at least plausible. Fourth, other experiments in our laboratories on Fe_n^+[15] and V_n^+[41] clusters yield CID thresholds that are much lower in energy (1.6–3.0 eV). This indicates that the high values determined here are not due to some experimental artifact. Clearly, further experiments will be useful understanding the disagreement here.

In agreement with these photodissociation studies, our results show that the dominant mechanism for dissociation of these clusters is the loss of a single Nb atom from the cluster ion. The coincidence in the fragmentation patterns suggests that both collisionally activated and photoexcited clusters proceed by the same reaction pathway, presumably rapid equilibration of energy into internal modes followed by dissociation to ground-state products. In Nb_4^+ CID, our data indicate that $Nb_2^+ + Nb_2$ are the dominant products at low energies, but that $Nb_3^+ + Nb$ are more probable at higher energies. Since Nb_3^+ was the primary product observed in the photodissociation of Nb_4^+, our results suggest the presence of highly energetic multiphoton processes in those experiments (or interesting differences in reaction dynamics for this cluster).

D. Dissociation Mechanism. In collision-induced dissociation of Nb_n^+, the lowest energy dissociation pathway is found to be $Nb_n^+ \rightarrow Nb_{n-1}^+ + Nb$, with the exception of $n = 4$. All smaller ionic cluster products are also observed, but with higher threshold energies. Near these thresholds, the product ions are accompanied by the largest molecular neutral products possible. At higher energies, smaller ionic products are also formed by fragmentation of the larger product ions. These reaction branches are evident as increases in the cross sections of decomposition products near the expected thermodynamic thresholds. Thus, in CID of Nb_n^+, sequential atom loss or "evaporation" and cluster "fission" occur readily to form all possible fragment ions and neutrals.

These observations are in agreement with the dissociation patterns of larger niobium clusters observed by CLR.[12,13] Note that photoionization and dissociation of Nb_4^+ was not included in those studies. Since the size ranges of our respective studies are not overlapping, more extensive comparisons are difficult to make. As we extend these CID experiments to include larger clusters, the combination of the various results should yield a more comprehensive picture of Nb clusters.

The occurrence of niobium cluster fission is in contrast to the fragmentation pattern observed for CID of small iron ion clusters.[15] Fe_n^+ ($n = 2$–10) clusters dissociate exclusively by sequential loss of Fe atoms. No evidence for fission of Fe_n^+ to molecular neutral products is observed over the same range of collision energies. One of the most obvious causes for this difference in fragmentation patterns is the difference in cluster bond strengths. The Fe_n^+ BDEs are about 2.5 eV, whereas Nb_n^+ BDEs average about 5.5 eV. However, the bond strengths of the neutral products appear to be more important in governing the fragmentation pattern. For iron, the neutral dimer bond is fairly weak, $D°(Fe_2) = 1.12 \pm 0.15$ eV. This apparently hampers efficient formation of Fe_2 and larger neutral iron fragments. On the other hand, the niobium

(38) Chase, M. W., Jr.; Davies, C. A.; Downey, J. R., Jr.; Frurip, D. J.; McDonald, R. A.; Syvrud, A. N. *J. Phys. Chem. Ref. Data* **1985**, *14*, sup 1, 1605.

(39) Freund, H. J.; Bauer, S. H. *J. Phys. Chem.* **1977**, *81*, 994.

(40) Levine, R. D.; Bernstein, R. B. In *Molecular Reaction Dynamics and Chemical Reactivity*; Oxford: New York, 1987.

(41) Hales, D. A.; Armentrout, P. B., work in progress.

neutral dimer is quite strongly bound compared to iron, $D°(Nb_2)$ = 5.2 eV, making formation of large neutral fragments possible.

The relative bond strengths of niobium and iron clusters may reflect fundamental differences in the bonding of these two metals. Nb–Nb bonds are much stronger than Fe–Fe bonds, and it seems reasonable to attribute this to multiple metal–metal bonds for Nb. Since Fe is on the right-hand side of the periodic table, its 3d orbitals are contracted compared to those of Nb. Consequently, Fe_n^+ cluster bonding is thought to have less d–d interaction and proportionately more 4s–4s bonding.[42,43]

Another possible reason for the difference in fragmentation patterns between these two metals is that Nb and Fe clusters have different structures. For instance, a linear chain of atoms might be expected to break apart into molecular fragments upon collision, producing ionic and neutral cluster moieties. In contrast, a nearly close-packed structure may prefer to dissociate by popping-off random atoms sequentially from the cluster. Unfortunately, there is no structural information available on Fe or Nb clusters, although isomers of Nb_n have been previously postulated to account for apparent two-component reaction rates for niobium clusters.[44,45]

In this study, Nb_n^+ with even numbers of atoms are found to be more stable than Nb_n^+ with odd numbers of atoms (Table II). The CID branching ratios of the clusters generally reflect these relative binding energies. At higher energies, where extensive fragmentation occurs, product ions with even numbers of atoms consistently have higher relative probabilities for formation. These branching ratios are especially evident in comparison of Nb_5^+ and Nb_6^+ CID (Figure 1, d and e). If we take the primary CID product (Nb_{n-1}^+) as a standard, the secondary product (Nb_{n-2}^+) is relatively favorable in CID of Nb_6^+, where the secondary product is Nb_4^+, than for CID of Nb_5^+ to form Nb_3^+. Similarly, the tertiary product (Nb_{n-3}^+) is relatively favored in Nb_5^+ CID, where the product is Nb_2^+, compared to Nb_6^+ where the tertiary product is Nb_3^+. The same branching ratio effect can be seen for the quaternary products.

(42) Shim, I.; Gingerich, K. A. *J. Chem. Phys.* **1982**, *77*, 2490.
(43) Leopold, D. G.; Almlof, J.; Lineberger, W. C.; Taylor, P. R. *J. Chem. Phys.* **1988**, *88*, 3780.
(44) Hamrick, Y.; Taylor, S.; Lemire, G. W.; Fu, Z.-W.; Shiu, J.-C.; Morse, M. D. *J. Chem. Phys.* **1988**, *88*, 4095.
(45) Zakin, M. R.; Brickman, R. O.; Cox, D. M.; Kaldor, A. *J. Chem. Phys.* **1986**, *88*, 3555.

V. Conclusions

We have shown that ion beam studies can provide a wealth of quantitative information on transition-metal clusters. In this work, both ionic and neutral binding energies are derived from CID cross section threshold analysis. These BDEs, in turn, yield the cluster ionization potentials. In these systems, the numerous CID product channels provide redundant and complementary information, such that a consistent set of thermochemical data is obtained. The qualitative cross section energy dependences and the relative energy thresholds furnish insight into the mechanisms of Nb cluster dissociation.

In the future, we plan to extend this study to larger Nb_n^+, which will also provide information on the neutral clusters, since the IPs of larger clusters are already known.[37] Because the IPs of these large clusters do not decrease monotonically, it will be interesting to see if the same fragmentation pattern is observed. Determination of quantitative information though is not limited to CID processes, but through application of these techniques to reactive systems, we expect to gain thermochemical, kinetic, and mechanistic information on chemical reactions of metal clusters. We anticipate that niobium clusters should be very interesting reactive species, because of the strong bonds that can be formed with other molecules and atoms and the strong bonds within the clusters themselves.

Acknowledgment. This work is supported by the Army Research Office, DAAL03-87-2211.

Registry No. Nb_2^+, 73145-87-6; Nb_3^+, 99775-01-6; Nb_4^+, 73145-88-7; Nb_5^+, 73145-89-8; Nb_6^+, 73145-90-1; Nb, 7440-03-1; Xe, 7440-63-3.

Orientational Analysis of Micelle-Associated Trehalose Using an NMR–Pseudoenergy Approach

Preetha Ram, L. Mazzola, and J. H. Prestegard*

Contribution from the Chemistry Department, Yale University, New Haven, Connecticut 06511.
Received July 15, 1988

Abstract: A combined NMR–pseudoenergy approach to conformational and orientational analysis is applied to trehalose, a disaccharide with known membrane surface associative properties. Trehalose is incorporated into a medium composed of discoidal cesium perfluorooctanoate micelles that order spontaneously in high magnetic fields, and NMR data in the form of deuterium quadrupole splittings and dipolar splittings for carbon–proton and proton–proton interactions are acquired in suitably deuterated molecules. Preferred orientations of trehalose relative to micellar surfaces are initially sought by searching for director axes that approximately satisfy all the experimental observations. The director orientation and molecular conformations are then optimized by a modified molecular mechanics program in which orientational information from both deuterium quadrupole splittings and dipolar splittings is represented by pseudoenergy terms added to the program's empirical description of molecular energies. By this approach it has been possible to find probable conformations and orientations for trehalose on the micellar surface.

Carbohydrates perform a variety of functions at the surface of biological membranes.[1] As glycoconjugates of lipids and proteins, they act as receptors for a number of hormones and toxins; they also contribute significantly to the structural integrity of membranes. As simple saccharides they participate in a number of metabolic functions and even aid in protection from severe environmental fluctuations. The disaccharide trehalose, for example, is believed to aid in protection of cell membranes from the effects of dehydration and freezing by extensive hydrogen bonding to the phospholipid headgroups.[2,3]

(1) Sharon, N.; Lis, H. *Mol. Cell. Biochem.* **1982**, *42*, 167–187.
(2) Crowe, J. H.; Crowe, L. M.; Carpenter, J. F.; Rudolph, A. S.; Wistrom, C. A.; Spargo, B. J.; Anchordoguy, T. J. *Biochim. Biophys. Acta* **1988**, *947*, 367–384.

0002-7863/89/1511-3176$01.50/0